

Adaptive Mesh Refinement and Turbulence Modeling

Michael E. Olsen*

Corresponding author: michael.e.olsen@nasa.gov

* NASA Ames Research Center, Moffett Field CA 94035-1000 USA

Abstract: Adaptive mesh refinement is shown to be essential in turbulence modeling. Adaptive Mesh Refinement (AMR) is a more computationally efficient means to obtain a discrete approximation to a continuous boundary value problem of a specified accuracy than classic isotropic grid refinement. Previous application of this methodology in the assessment of turbulence models suggested that the field variable solution on the interior of the domain was more sensitive to grid refinement than would be suggested by the sensitivity to grid refinement of surface quantities. Revisiting challenging high speed flow field revealed that anomalous predictions aspects believed to be fundamental turbulence model issues appear to be related to an under-resolved boundary layer edge – a flow detail previously considered unimportant.

Keywords: Numerical Algorithms, Computational Fluid Dynamics, Turbulence Modeling, Adaptive Mesh Refinement.

Nomenclature

List of Symbols

θ	flare cone angle
T	static temperature
p	static pressure
c_v	(constant) specific heat at constant volume
e_i	internal energy $\int_0^T c_v dT' = c_v T$
h_t	total enthalpy $e_i + p/\rho + k + \frac{1}{2}(u * u + w * w)$
k	turbulent kinetic energy (per unit mass), $\frac{1}{2}\overline{u'_i u'_i}$
\dot{q}_w	wall convective wall heating
\overline{u}_i	ensemble mean velocity in i direction
ν_t	kinematic eddy viscosity
ρ	mass density
u	mean axial velocity
w	mean radial velocity

List of Subscripts

∞	reported experimental conditions upstream of interaction
w	evaluated at wall

1 Introduction

The computational grid is fundamental to the quality of any discretized solution of a fluid dynamics problem. Rules of thumb, best practices guidance, and bitter previous experience are all helpful in the creation of a reasonable quality grid. Having a system which can improve such a grid to provide adequate resolution of flow features that depend on the solution itself makes it possible, in principle, to obtain arbitrarily accurate simulations starting with a reasonable baseline grid system.

Mesh refinement reduces the truncation error of a solution. Adaptive mesh refinement (AMR) refines subregions of the solution domain based on a heuristic sensor (e.g. vorticity), solution of an adjoint equation, or in the method employed in this paper, a measure of the extent to which the solution may be represented as a linear function on the current grid.

One benefit of AMR is that grid-converged solutions may be obtained with much lower memory requirements since only flow regions that require grid refinement incur the additional computational cost of solving on a finer grid. Another is that the error can, in principle, be reduced to an arbitrary level. In assessing turbulence model behavior, this essentially allows the analyst the ability to obtain the predictions of a given turbulence model without the confounding effects of discretization error.

2 Problem Statement

Previous work [12] suggested that velocity profile predictions in high speed flows might require much more grid resolution than previously thought. In that paper, the surface quantities, both pressure and skin friction, were surprisingly insensitive to the additional refinement, while the field variables were still not completely grid-converged. This is a useful attribute when utilizing turbulence models for vehicle design, but it also implied that convergence of surface quantities was not sufficient to guarantee that the flowfields were adequately resolved if turbulence model development was the design task. The real point of that work, however, was the discussion and exploration of an algorithm to use of AMR to obtain an arbitrarily accurate approximation to the "exact" solution for a given flowfield case.

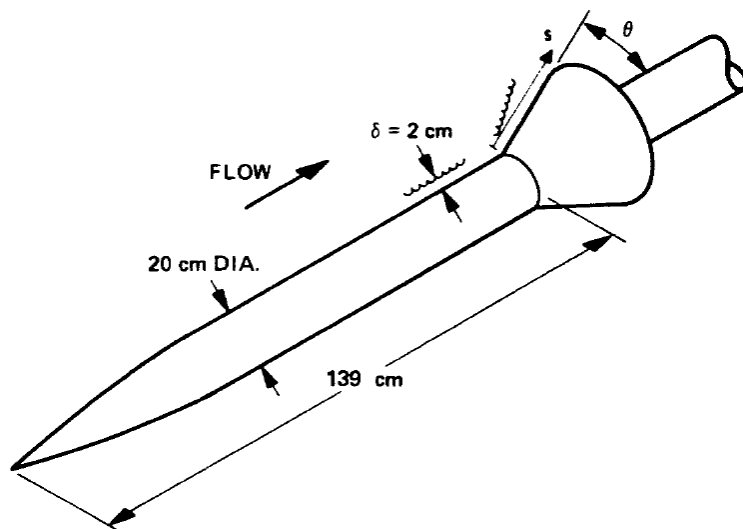


Figure 1: Test Article Geometry

With this new recipe for the use of OVERFLOW's AMR in hand, a grid converged solution, to a previously run, and already reported case [11] was desired, merely to confirm that the previously reported result was indeed grid-converged: the $M_\infty = 7$ cylinder-flare case of Kussoy [10]. Surprisingly for all cylinder flare angles in that dataset, there were differences, and most importantly, the solution for the largest flare angle (35°), which exhibits the largest separation, had surface pressures (along with the more sensitive wall heating, and velocity profile) which were significantly different from those previously reported.

2.1 Experimental Conditions

The case considered here is the Kussoy and Horstman hypersonic cylinder-flare case [10], with the underlying cylinder model described more completely in [9]. This flowfield has been considered previously in [11, 14, 8]. An 8-inch (0.2032 m) diameter

cylinder flare, with a coe-ogive nose and cone flares of 4 conical angles were tested in the Ames 3.5-foot hypersonic wind tunnel (Fig. 1). Inflow conditions just upstream of the interaction region are given as:

$$\begin{aligned}
 M_\infty &= 7.04 & u_\infty &= 1127 \text{ m s}^{-1} & T_w &= 311 \text{ K} \\
 T_\infty &= 81.2 \text{ K} & p_\infty &= 576 \text{ Pa} & \tau_{w_\infty} &= 25 \text{ Pa} \\
 \rho_\infty &= 0.02522 \text{ kg/m}^3 & Re &= 5.8 \times 10^6 \text{ m}^{-1} & \dot{q}_{w_\infty} &= 9300 \text{ W/m}^2
 \end{aligned}
 \tag{1}$$

It is implicitly assumed, and confirmed by computation, that the inflow conditions at this station (for the cases and turbulent models that are fully attached at that point, 6 cm upstream of the beginning of the flares) are identical for all cone-flare cases.

The experimental facility was a pebble-bed heated blow down facility capable of high Reynolds number flows at high Mach numbers. The test article was injected into the flowfield after the tunnel came to condition, allowing the heating as well as the surface pressure to be measured in the test campaign. Four cone angles were studied, with the smallest, $\theta = 20^\circ$, an essentially attached flow. This anchors the validation efforts, providing a case that does not require the turbulence model to be capable of predicting flow separation. The next highest case $\theta = 30^\circ$ has a small separation at the cylinder/cone intersection, while the next two cases increase the conical angle, and the extent of the separation.

The test article entered the flowfield downstream of the contoured nozzle, and the nozzle presumably had some weak compression or expansion waves at the nozzle lip, which was 3.5ft (1.0668 m) in diameter, and the test article is 1.4m in length before the start of the conical flare. It is assumed that the entire test article is contained within the "test diamond" of the nozzle/test section, and is roughly a uniform flowfield into which the cone/ogive/flare is stationed.

Having run these cases and obtained what are essentially grid-converged results for the oncoming flow, there are interesting issues that become apparent looking at the results, one of which is (apparently) the reflection of the expansion fan from the ogive reflecting off the conical shock created by the nose, creating a very small compression wave very close to the "reference location", 6cm upstream of the cylinder-flare intersection. However, the pressure perturbation created is reasonably small, but quite visible in the detailed surface pressure plots of the fully grid-converged solutions for all turbulence models studied.

A more important issue came to light when the author rescued the actual test article from being scrapped. The surface finish was found to be quite rough, as was apparently typical of models tested in the facility. All these cases have been simulated using smooth wall boundary conditions, but this does highlight an issue that merits documentation for experimental test programs that are potentially suitable for turbulence model and/or code validation, or for others simulating this flowfield.

2.2 Baseline Grid and Solution Domain

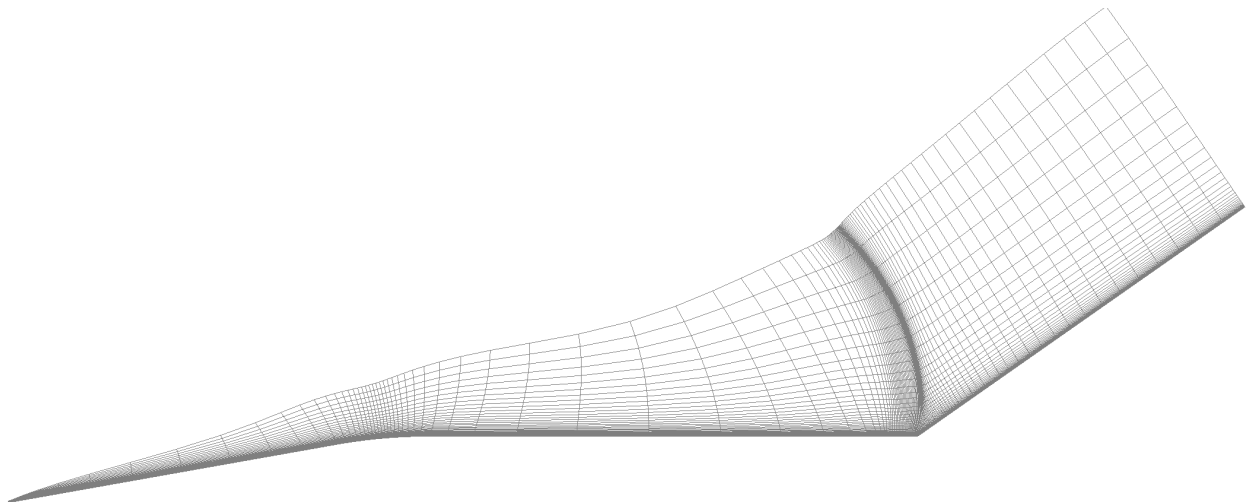


Figure 2: Baseline Grid System (every 3rd × 4th grid line shown)

The baseline grids for these cases were based on the original grids [11], except that the axial spacing was greatly diminished, with the aim of obtaining grid-converged results with a much more efficient grid system than the original classic grid refinement strategy. The base grid system was $352(\text{axial}) \times 257(\text{radial})$, with an initial radial spacing of 1×10^{-6} m, and roughly constant stretching of 1.035. No grid tailoring to fit the shock was done for this grid system, and using the Chimera Grid tools [6] programs HYPGEN and SETZETA, the grid was extended far enough to comfortably contain the external shock.

It is worth noting that the hope for obtaining substantially better computational efficiency was not uniformly realized as the first two grid refinement levels were nearly equivalent to simple classic mesh refinement in terms of grid point count, but as can be seen from Fig. 2, the grid was more nearly isotropic at a good part of the farfield, where the original grid might have been more axially dense. The subsequent refinement levels did exhibit more computational efficiency, however, with roughly a doubling of grid count rather than a four-fold increase with each additional level.

2.3 Turbulence Models

The predictions of three turbulence models were compared. Only one of these three is unchanged from the previous work, the Lag- ν_t model, which has not changed from the version described in [11]. The SST and SA models have both been altered from the versions from that work(using the stock OVERFLOW 2.0s), but were verified by the author to be consistent with the descriptions in [1]. The SA model and SST model used in this work are from the standard 2.2k OVERFLOW distribution, which were verified [7] to be coded to consistently with the description on the turbulence modeling resource website [15]. The SA model was run in the way as recommended by Spalart [13], with the rotation correction. The only adjustment to the SST model was run with vorticity production, but comparison with strain based production did not make discernible differences on the baseline grid.

2.4 Simulation Methodology

These cases were simulated using a modified version of OVERFLOW2.2k [2]. The chosen numerical scheme was identical to that of [11], with matrix dissipation, and the Pulliam-Chausee algorithm. The adaptive mesh refinement [4, 5, 3] capabilities of OVERFLOW were used in the same manner as previously reported [12], which studied three validation flowfields: subsonic, transonic, and supersonic. Similarly, the second undivided difference sensor is employed,

$$S = \max_{i=j,k,l} \left\{ \max_{q=[\rho,\rho u,\dots]} \left[\left(\frac{q_{i-1} - 2q_i + q_{i+1}}{2q_{ref}} \right)^2 \right] \right\} \quad (2)$$

where $q = [\rho, \rho u, \rho v, \rho w, \rho e_0]$, the conservative mean variables at each grid point, and the $i = [j, k, l]$ indices denote the computational space indices in the Steger convention. The reference divisors for these variables are $q_{ref} = [\rho_\infty, \rho_\infty u_\infty, \rho_\infty v_\infty, \rho_\infty w_\infty, \rho_\infty e_{t_\infty}]$. The turbulence field variables are also added to this mix, with the exception of the ω equation for the SST and Lag- ν_t models. This function is a measure of the linearity of the solution. It is the ratio of the 2nd derivative of the conservative variables (without the associated grid metrics) in computational space to their freestream magnitude. This goes to zero as the grid is refined and linear interpolation is a better and better approximation of the solution between grid points. Further detail is described in [12], but can be quickly sketched as a recursive process in grid refinement level. Starting with a fully (relaxation method) converged solution on the fully (AMR method converged) grid system, the AMR is asked to refine the solution one level finer till the number of grid points ceases to grow with refinement passes. At this point the solution is then run more relaxation iterations to completely converge the solution on the grid system obtained by this process to yield the relaxation and AMR method converged solution at the next level.

The experience for the supersonic case in [12] is consistent with what was found in this hypersonic case, except that for this case, the effect of the mesh refinement was far more dramatic.

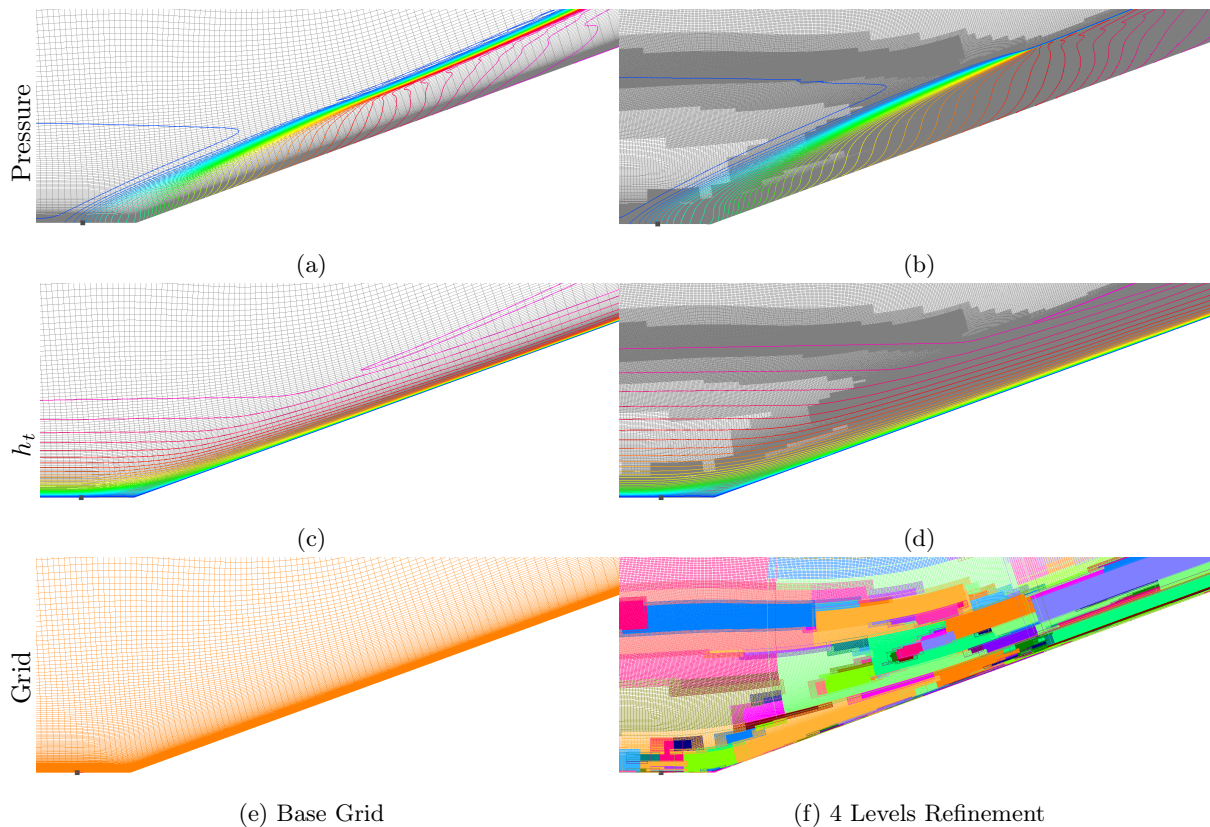


Figure 3: Pressure field and grid in shock/boundary-layer interaction region

3 Results

3.1 Attached case: $\theta = 20^\circ$

Figure 3 shows some of the details of the solution for the nominally attached case ($\theta = 20^\circ$) in the cylinder flare intersection region. Figures 3a and 3e shows the pressure field and grid system of the solution obtained on the original unrefined grid. The small symbol visible on the bottom of the solution domain is a point that is essentially at the reference condition, 6 cm upstream of the cone-flare intersection. Figures 3b and 3f show the same region after four levels of refinement. Each different color patch shown in Fig. 3f is a region that has been further refined, with the finer grid replacing the underlying coarser grid at that location. These finer patches will have even finer patches replacing portions of the domain with even finer mesh regions, so that at the regions that have been refined at the finest level, there are 6 patches overlaying each other at those physical regions. This process produces the colorful abstract (Cubist, or Hexahedrist?) painting of the solution region shown in Fig. 3f.

There are regions that remain at a low level of refinement as the AMR process proceeds. The mesh refinement parameters are set to tend to keep an area refined which has already been refined, so these coarser grid regions in the domain are regions that have smaller solution variation than the surrounding region through the entire solution/grid refinement process.

However, the solution for the pressure field away from the wall is substantially different for the highly refined grid system, as is most easily seen in the region near the cylinder/flare intersection. The more refined grid system has a substantially higher region of enhanced pressure, and the compression waves emanating from the separated region which coalesce with the other compression waves emanating from further downstream produce a much more complex shock shape in the highly resolved grid system. But note that the compression waves are building up to what appears to be a well-defined shock at the upper right of the domain, but they are building to that shock as we move from the cone flare intersection up the flank of

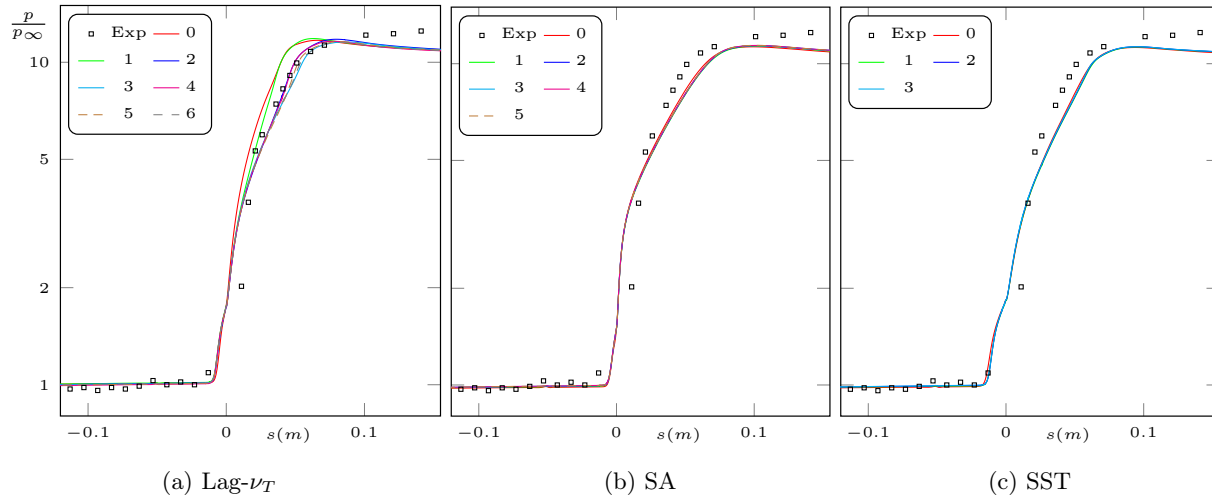


Figure 4: Surface pressure, legend refinement level, $\theta = 20^\circ$

the cone. The baseline grid is not capable of representing this subtle feature.

Figures 3c and 3d show the total enthalpy field for this flowfield which highlights the tendency of the AMR method to refine the boundary layer edge. Normally, this additional flow detail is completely inconsequential to the inner boundary layer predictions, but in this case, the more well-defined enthalpy field in the outer edge of the boundary layer feeds directly into the flowfield that develops on the conical flare flowfield. There is an interaction between the enthalpy and the pressure field where the upstream boundary layer is impinging on the boundary layer developing on the conical flare.

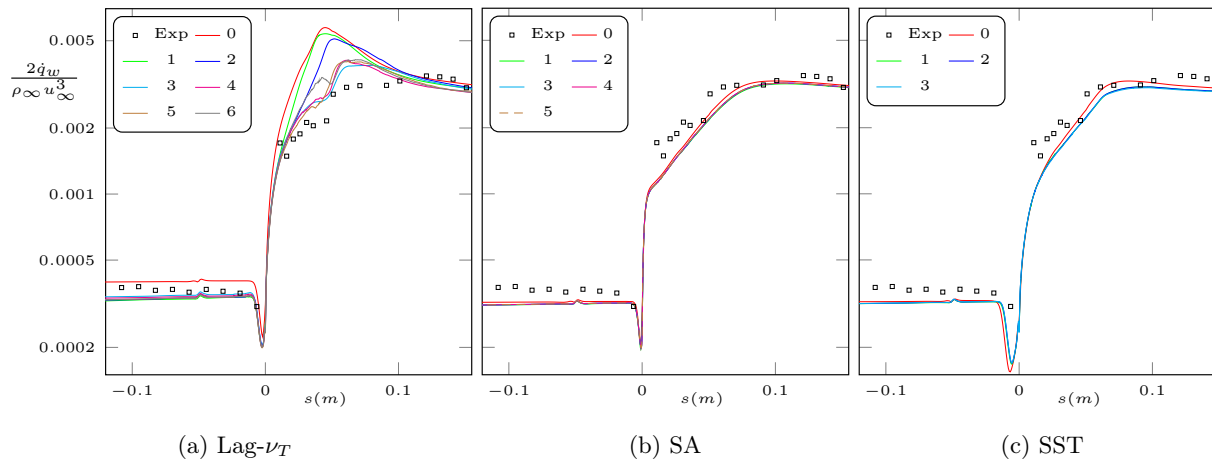


Figure 5: Surface heating comparisons, $\theta = 20^\circ$

Looking at the surface pressures (Fig. 4), differences made by what are significant flowfield differences are relatively small. Wall heating results (Fig. 5) were actually a bit of surprise. Where previous results showed little variation with grid density, the flare heating results are significantly changed by the adaptive mesh refinement strategy, at least for the Lag model. One area that the AMR always refines in flows with boundary layers, at least in this authors experience, is the boundary layer edge. For attached flows, this is generally of no consequence, and seems to make no appreciable difference deeper in the boundary layer. However, for this case, even though it is attached, resolving the boundary layer outer edge may explain these heating differences on the conical flank, much like resolving that edge could affect multi-element airfoil flows,

where the wake of one device is the upstream state for another. The peak in heating seen in the coarsest grid was a far more persistent phenomenon on the traditionally refined grids, but it is the case that even in the finest grid system, the outer boundary layer edge was not well resolved, based on normal gridding practices.

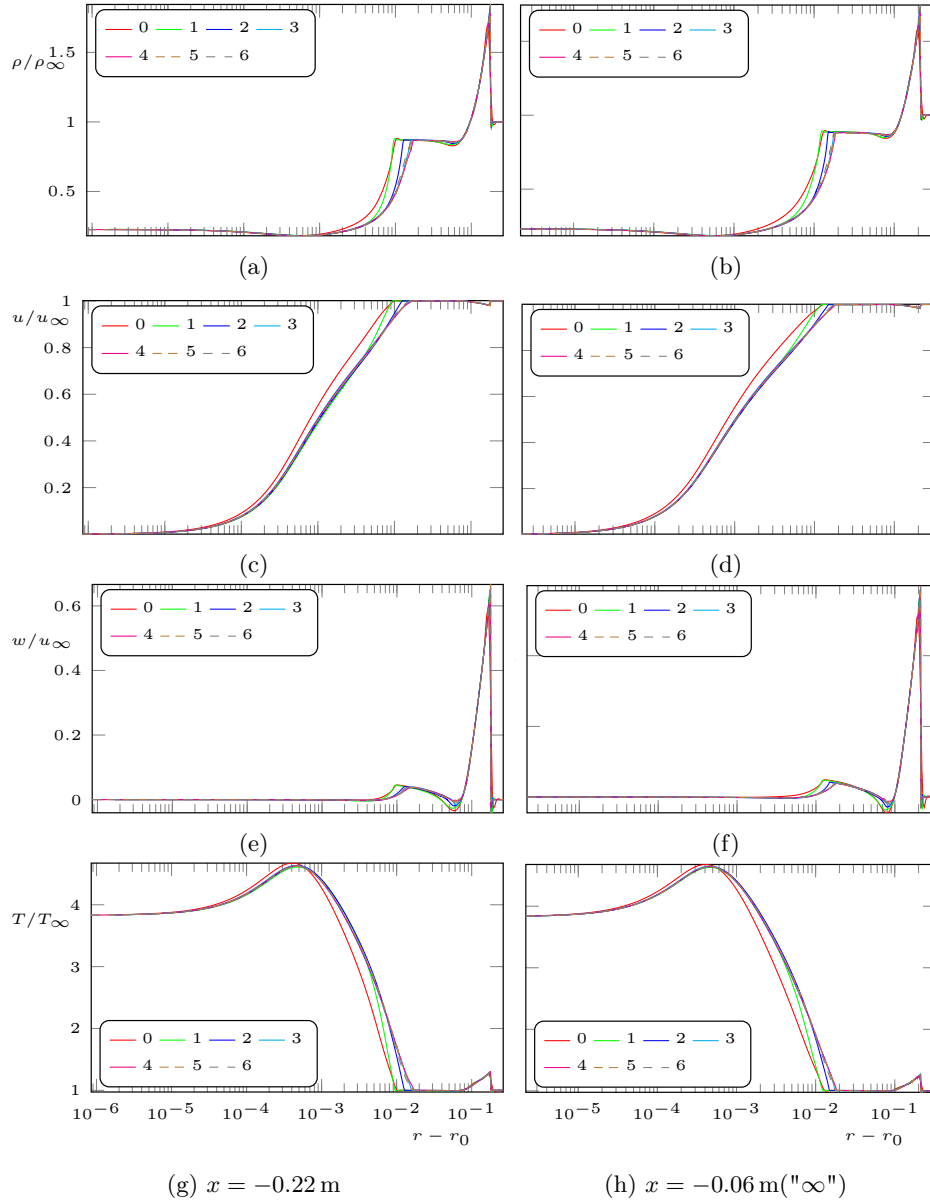


Figure 6: Mean flow state upstream of interaction region (Lag model)

third and higher refinement.

More quantitatively than these pictures, however, what does the mean flow state upstream look like with grid refinement for this grid system? Recall that this is nominally the same state for all cone flare angles, so investigation for the $\theta = 20^\circ$ is relevant for all flare/cone systems. It also has the benefit of having no separated flow at the reference location at roughly 6 cm upstream of the cone/flare intersection, unlike the highest flare angle case, as is evident in the pressure field from the experiment. Figure 6 shows the state well upstream of the interaction region, and at the reference location. It is roughly borne out that the baseline and first refinement level have not reached grid independence, but that the second refinement level and above are yielding essentially the same mean inflow state (mass, momentum and energy). The regions where changes are occurring upstream in the first three refinements are mainly at the boundary layer edge(approximately 2 cm from the

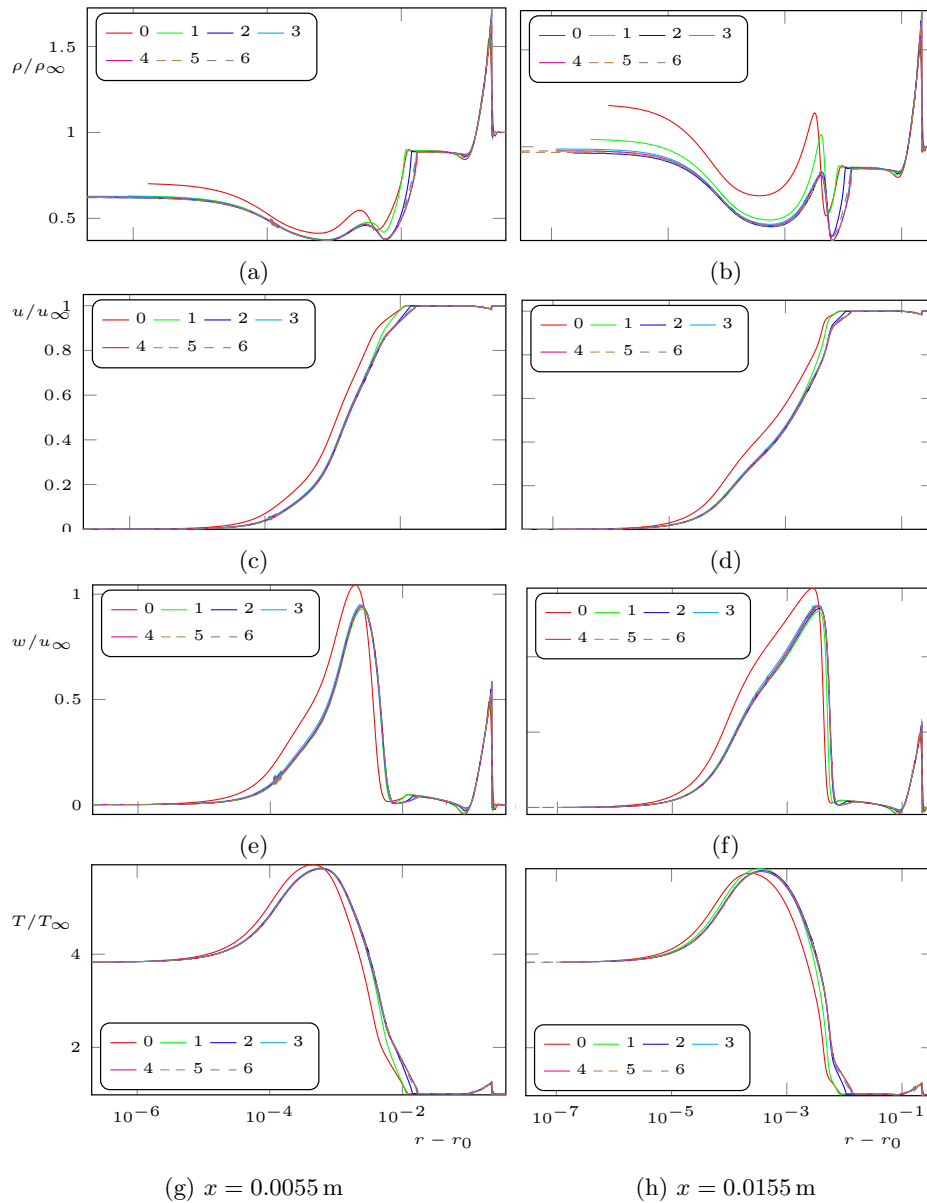


Figure 7: Mean flow state downstream of interaction region (Lag model)

eventually coalesce into a shock (Fig. 3b).

Downstream of the interaction region, the situation is more complex, as might be expected from the pressure field differences noted in Fig. 3. Similar to what was seen in the upstream profiles, the mean flow state downstream of the cone-flare intersection is largely done changing with the third level of refinement. However, where in the upstream profiles, the changes with grid refinement were largely confined to the boundary layer edge, the downstream profiles in Fig. 7, exhibit significant differences throughout the entire boundary layer. Density (Fig. 7a) has significant differences throughout the boundary layer, especially at the furthest downstream region plotted.

A plausible explanation of what is occurring is the better resolved upstream boundary layer edge flowing onto the flare (Fig. 6 makes significant differences in the entire boundary layer on the flare by changing the way the compression waves interact emanating from the surface and

3.2 Fully separated case: $\theta = 35^\circ$

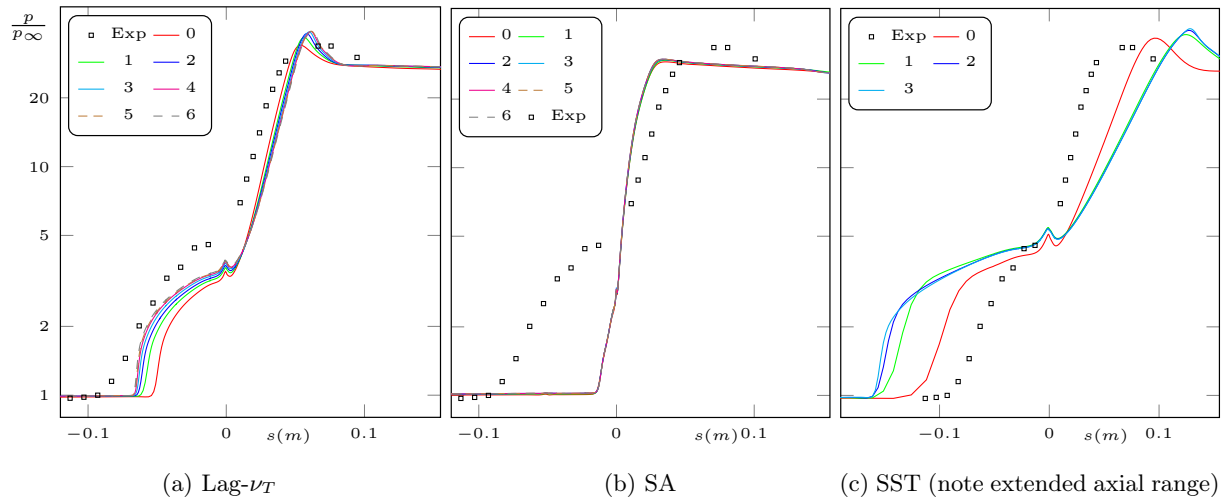


Figure 8: Surface pressure comparisons, $\theta = 35^\circ$

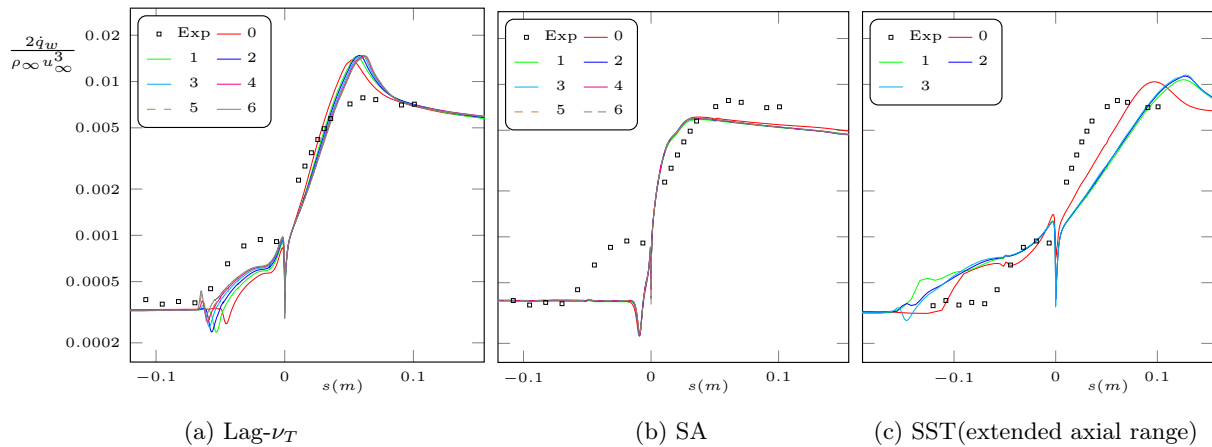


Figure 9: Surface heating comparisons, $\theta = 35^\circ$

The most intriguing case here is the one which none of the models were able to predict in the 2005 paper [11]. Surface pressures for this case are shown in Fig. 8, where now with the enhanced grid resolution allowed with AMR in play, the separation region is much better predicted by the Lag model. The other eddy viscosity models respond differently, with SA seemingly unaffected by grid refinement, but SST responding with larger and larger spurious separations.

This case has the same inflow conditions as the previously discussed 20° case, so the same differences in inflow conditions to the interaction region are in play for this case also, here for the Lag model turning the one case that did not agree well with experiment much more in line with the separation extent. The heating downstream of re-attachment decreases with finer grids, moving closer to the experimental values, where in the previous work, additional grid refinement made for more disagreement.

Now that we appear to have a system that can provide solutions that are grid-independent, we can investigate some uncertainties in the experimental data set. One of these that is instructive for this case is the location of transition. All cases presented so far are for fully turbulent simulations. To assess the possible influence of a region of laminar flow on the nose, simulations were made with the transition occurring just

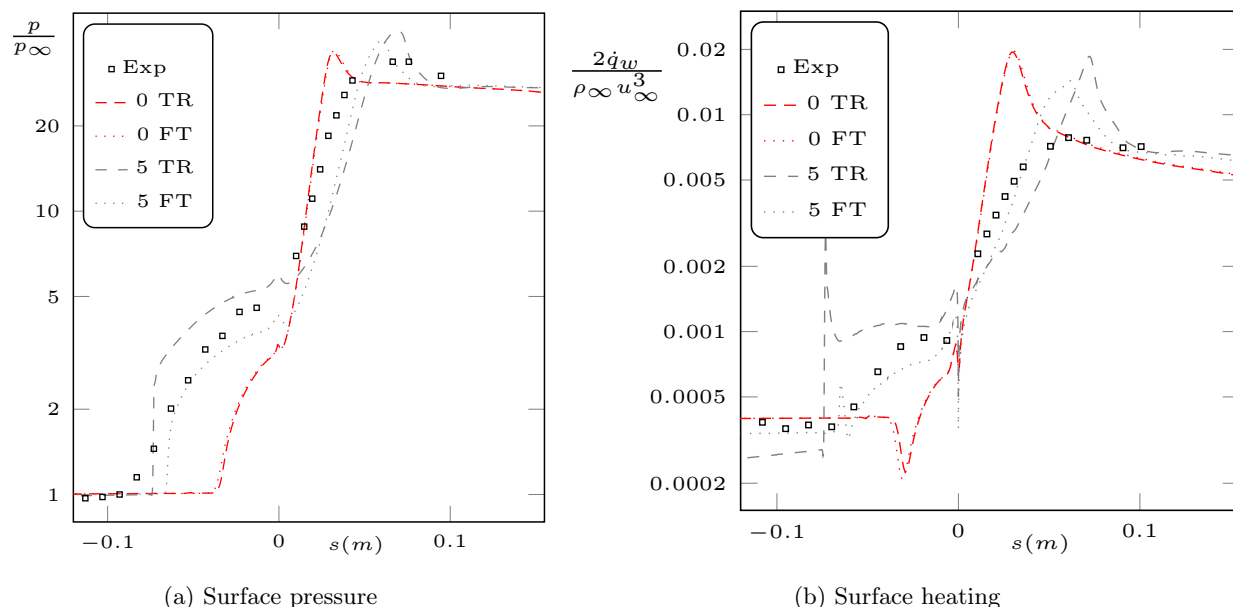


Figure 10: Transition assessment, Lag model (FT≡"Fully turbulent", TR≡"Transitional"), $\theta = 35^\circ$

downstream of the front ogive/cylinder intersection, which is far further downstream than was likely possible, but it should bound the effect. The surface pressure and heating for this case with the Lag model are shown in Fig. 10. The less fully developed boundary layer results in a more extensive separation — larger than seen in experiment. It also misses the upstream heating (for the fully resolved grid system), suggesting that the fully developed simulations are closer to the actual experimental conditions. More troubling, however, for turbulence model development, is the predicted lack of influence of transition location on the predictions in the baseline grid system. Looking at these results, the effects of a large laminar extent on the nose would have been deemed not a significant uncertainty.

That transition location now has a significant influence is just one example of turbulence model parameters and experimental details that showed little effect on the baseline grid, and have subsequently been found to have effects on the more refined grid. The better resolved outer upstream boundary layer edge details now directly affect the flow throughout the boundary layer of the flare region. The amount of additional grid resolution is still, even with AMR, quite substantial, but there seems to be good reason for this sensitivity. In the case of transition, that directly affects at least one directly relevant parameter, the boundary layer thickness. In terms of turbulent model parameters, those that affect the turbulent/non-turbulent interface (like the turbulent transport terms) are another example.

4 Conclusion and Future Work

Turbulence models were tuned and evaluated using grids that were thought to be sufficiently fine. With a tool where reaching arbitrarily fine solutions is possible; and where pre-conceived notions of what is important can be challenged by accurate solutions of the entire boundary value problem, this assessment is being revised. Even for the attached flow case, there is a significant improvement in one of the issues associated with the heating on the flare, that might be associated with, among other things, insufficient grid resolution in the outer boundary layer region. In the most massively separated flow case of this set, the improvement provided by adaptive meshing showed the previous result was partially due to a insufficiently resolved grid. With the ability to provide much better answers, more subtle model tuning will be possible. Even with the efficiencies of AMR, the fully resolved grid systems are much larger than would have been contemplated before, but the additional resolution is targeted in the regions where it is needed to provide a truly grid independent solution.

More advanced versions of the SA model (specifically QCR) may improve its predictions. Tuning of

the SST model with Menter's new adjustable model strategy is also worth pursuing. For the Lag model, comparison with other high-speed flow cases is anticipated for the eddy viscosity model. The more advanced turbulent transport (TTR) Lag models terms give better boundary layer edge state predictions of the actual turbulent field. Given the improvement seen in the heating in the attached case, this is also worth investigating in these high speed flowfields.

References

- [1] Bardina, J. E., Huang, P. G., and T.J. Coakley. Turbulence Modeling Validation, Testing, and Development. Technical report, April 1997. NASA TM 110446.
- [2] P Buning, D Jespersen, T Pulliam, G Klopfer, W Chan, J Slotnick, S Krist, and K Renze. *OVERFLOW User's Manual, Version 1.8s*. NASA Langley Research Center, 2000.
- [3] Pieter Buning and Thomas Pulliam. *Cartesian Off-Body Grid Adaption for Viscous Time-Accurate Flow Simulations*. Fluid Dynamics and Co-located Conferences. American Institute of Aeronautics and Astronautics, Jun 2011.
- [4] Pieter G. Buning and Thomas H. Pulliam. *Near-Body Grid Adaption for Overset Grids*. AIAA AVIATION Forum. American Institute of Aeronautics and Astronautics, Jun 2016.
- [5] Buning, P. G. and Pulliam, T. H. Cartesian Off-Body Adaption for Viscous Time-Accurate Flow Simulations. AIAA Paper 2011-3693, June 2011.
- [6] Chan, William M. The OVERGRID Interface for Computational Simulations on Overset Grids. AIAA Paper 2002-3188, June 2002.
- [7] Childs, Marissa L., Pulliam, Thomas H., and Jespersen, Dennis C. OVERFLOW Turbulence Model Resource Verification Results. NAS Technical Report 2014-03, NASA, June 2014. NAS Technical Report NAS-2014-03.
- [8] Nicholas J. Georgiadis, Christopher L. Rumsey, and George P. Huang. *Revisiting Turbulence Model Validation for High-Mach Number Axisymmetric Compression Corner Flows*.
- [9] Kussoy, M.I. and Horstman, C.C. An Experimental Documentation of a Hypersonic Shock-Wave Turbulent Boundary Layer Interaction Flow – with and without Separation. Technical report, February 1975. NASA TM X 62,412.
- [10] Kussoy, M.I. and Horstman, C.C. Documentation of Two and Three-Dimensional Hypersonic Shock Wave/Turbulent Boundary Layer Interaction Flows. Technical report, January 1989. NASA TM 101075.
- [11] Michael Olsen, Thomas Coakley, and Randolph Lillard. *The Lag Model Applied to High Speed Flows*. American Institute of Aeronautics and Astronautics, Jan 2005. AIAA Paper 2005-101,.
- [12] Michael E Olsen and Randolph P Lillard. Using adaptive mesh refinement to study grid resolution effects for shock-boundary layer interactions. In *2018 Fluid Dynamics Conference*, page 3858, 2018.
- [13] Boeing(retired) Philippe Spalart. Personal communication. 2019.
- [14] Christopher Roy and Frederick Blottner. *Review and Assessment of Turbulence Models for Hypersonic Flows: 2D/Asymmetric Cases*.
- [15] Christopher Rumsey. Langley research center turbulence modeling resource, March 2015. [Online; accessed 6-May-2016]<http://turbmodels.larc.nasa.gov/>.